UNIVERSITÀ DI PARMA
ARCHIVIO DELLA RICERCA

University of Parma Research Repository

Permeation of Proteins, Oligonucleotide and Dextrans Across Ocular Tissues: Experimental Studies and a Literature Update

This is the peer reviewd version of the followng article:

Original
Permeation of Proteins, Oligonucleotide and Dextrans Across Ocular Tissues: Experimental Studies and a Literature Update / Pescina, Silvia; Govoni, Paolo; Antopolsky, Maxim; Murtomäki, Lasse; Padula, Cristina; Santi, Patrizia; Nicoli, Sara. - In: JOURNAL OF PHARMACEUTICAL SCIENCES. - ISSN 0022-3549. - 104:7(2015), pp. 2190-2202. [10.1002/jps.24465]

Availability:
This version is available at: 11381/2808206 since: 2021-10-19T11:51:18Z

Publisher:
John Wiley and Sons Inc.

Published
DOI:10.1002/jps.24465

Terms of use:

Anyone can freely access the full text of works made available as "Open Access". Works made available

Publisher copyright

note finali coverpage

(Article begins on next page)

12 October 2024

DOI: 10.1002/jps.24465

RESEARCH ARTICLE

Pharmaceutics, Drug Delivery and Pharmaceutical Technology

RESEARCH ARTICLE

Permeation of Proteins, Oligonucleotide, and Dextrans Across Ocular Tissues: Experimental Studies and a Literature Update

SILVIA PESCINA[1], PAOLO GOVONI[2], MAXIM ANTOPOLSKY[3], LASSE MURTOMÄKI[4], CRISTINA PADULA[1], PATRIZIA SANTI[1] AND SARA NICOLI[1]

[1]Department of Pharmacy, University of Parma, Parma 43124, Italy

[2]Department of Biomedical, Biotechnological and Translational Sciences, University of Parma, Parma 43126, Italy

[3]Centre for Drug Research, University of Helsinki, Helsinki FI-00014, Finland

[4]Department of Chemistry, Aalto University, Aalto FI-00076, Finland [Query:PE-Q1 to ALL] AU: Please check authors' affiliations and correspondence details for correctness.

Correspondence to: Sara Nicoli (Telephone: +39-0521-905065; Fax: +39-0521-905006; E-mail: sara.nicoli@unipr.it)

Received: 2015-01-09; Revised: 2015-04-02; Accepted: 2015-04-02

Proteins and oligonucleotides represent powerful tools for the treatment of several ocular diseases, affecting both anterior and posterior eye segments. Despite the potential of these compounds, their administration remains a challenge. The last years have seen a growing interest for the noninvasive administration of macromolecular drugs, but still there is only little information of their permeability across the different ocular barriers. The aim of this work was to evaluate the permeation of macromolecules of different size, shape, and charge across porcine ocular tissues such as the isolated sclera, the choroid Bruch's membrane and the cornea, both intact and de-epitelialized. Permeants used were two proteins (albumin and cytochrome C), an oligonucleotide, two dextrans (4 and 40 kDa), and a monoclonal antibody (bevacizumab). Obtained data and its comparison with the literature highlight the difficulties in predicting the behavior of macromolecules based on their physicochemical properties, because the interplay between the

charge, molecular radius, and conformation prevent their analysis separately. However, the data can be of great help for a rough evaluation of the feasibility of a noninvasive administration and for building computational models to improve understanding of the interplay among static, dynamic, and metabolic barriers in the delivery of macromolecules to the eye.

Keywords

macromolecular drug delivery; *in vitro* models; passive diffusion/transport; permeability; proteins; oligonucleotides; diffusion; monoclonal antibody

INTRODUCTION

Macromolecular drugs, such as proteins and oligonucleotides, represent nowadays important therapeutic tools in the treatment of ocular diseases. For instance, bevacizumab (149 kDa), ranibizumab (48 kDa), pegaptanib (50 kDa), and aflibercept (115 kDa) are currently in use (approved or off-label) for the treatment of neovascularisation in both anterior and posterior segment eye diseases; CNTF (ciliary neurotrophic factor, 23 kDa) is in clinical trial for the treatment of dry-AMD (Phase III) and retinitis pigmentosa (Phase II).[1] Several other proteins are under investigation,[2, 3] as well as oligonucleotides and other nucleic acids, as the inhibition of gene expression also represents a valuable therapeutic option for the treatment of diverse ocular pathologies for both the anterior[4] and posterior segment.[5] It is possible to expect that the understanding of the molecular basis of the pathologies will further increase the number of possible drug candidates in next years.

Drug administration to the eye is a difficult task because of the peculiar structure of this organ and the presence of static and dynamic barriers protecting the internal tissues. Presently, drug bioavailability to the anterior chamber after topical application is very limited (lower than 5%) because of the short residence time of the formulation on the ocular surface and the very low permeability of the cornea. Cornea consists of an external epithelium, a collagenous layer (stroma), and an internal endothelium (Fig. 1). The posterior segment of the eye is even more difficult to target: topical application is not efficient and systemic administration is hindered by the presence of the blood–retinal barrier. Bioavailability problems related to the posterior segment make the intravitreal injection the present option for drug administration. However, many studies are ongoing to evaluate the trans-scleral route as a possible noninvasive alternative to target the posterior segment. In this case, to reach the retina, drugs must diffuse across the sclera, choroid, Bruch's membrane, and retinal pigmented epithelium (RPE) (Fig. 2).

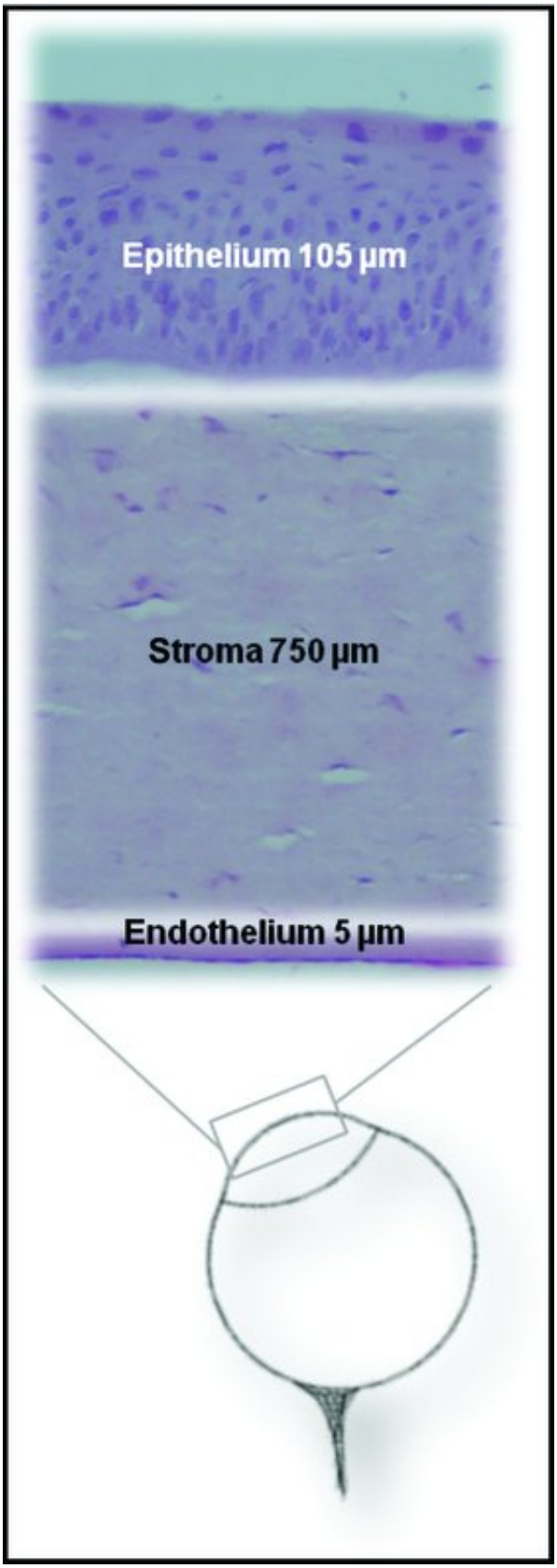

Figure 1 [Query:PE-Q1 to ALL] AU: Please check the presentation of the captions of Figures 1–9 for correctness. Schematic representation of the barriers involved in the permeation across the cornea. The outermost layer is the epithelium, followed by a connective tissue (stroma) and endothelium. The image is not to scale. The thickness reported is relative to porcine tissues.

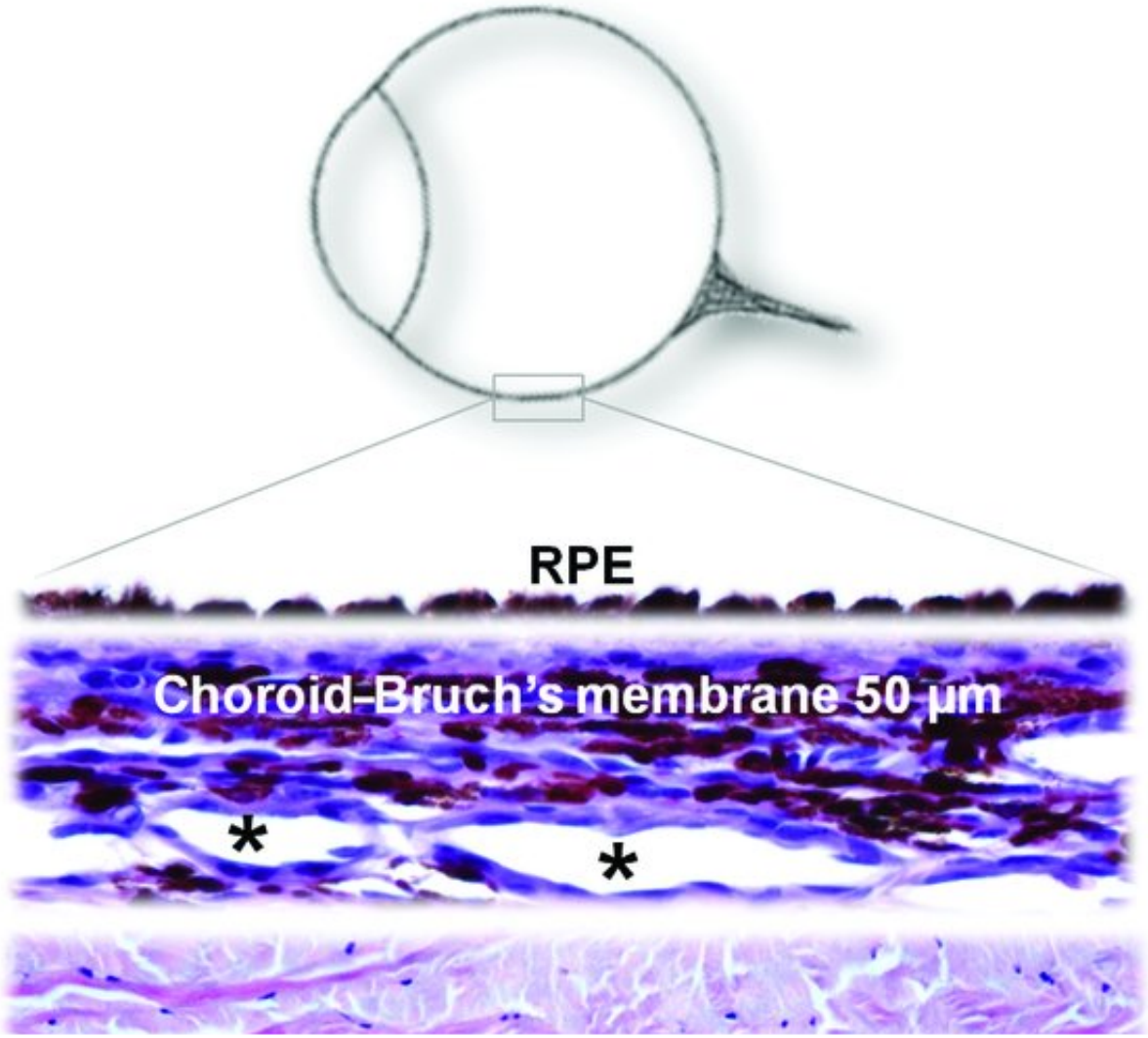

Figure 2 Schematic representation of the static barriers involved in trans-scleral permeation. The drug have to diffuse first across the sclera (connective tissue), then across the choroid (vascular tissue) and the Bruch's membrane to reach the RPE, a pigmented monolayer characterized by tight junctions and representing the outermost layer of the retina. The image is not to scale. The thickness reported is relative to porcine tissues. Asterisks indicate choroidal blood vessels, where a dynamic clearance

mechanism is present. The thickness reported is relative to porcine tissues.

Many papers on permeability of ocular barriers toward small drugs have been published, in order to understand how physicochemical characteristics such as the molecular weight (MW), lipophilicity, and ionization can impact on the flux.[6] Permeability data are of utmost importance as it provides the basis for the development of *in silico* models, which are crucial for predicting the rate of drug delivery to the eye and ocular bioavailability.[7-10] One of the problems in the building and validation of *in silico* models for macromolecules is the lack of an extensive collection of their permeability data. Such a collection should be based on data obtained from several laboratories and for macromolecules with a wide range of physicochemical properties.

The aim of this work was to evaluate the permeation of macromolecules of different size, conformation, and charge across porcine ocular tissues, in order to collect data of the molecular characteristics impacting their permeation. In particular, the isolated sclera, the bilayer choroid Bruch's membrane (CH-BM), and the cornea will be studied as barriers. As some corneal pathologies compromise the integrity of the corneal epithelium, permeation across de-epithelialized cornea will also be performed. Permeants used will be two model proteins (albumin, 66 kDa and cytochrome C, 12.4 kDa), a model oligonucleotide (7.9 kDa), two dextrans (4 and 40 kDa), and bevacizumab (149 kDa), a monoclonal antibody with the therapeutic rationale. The accumulation of bevacizumab and oligonucleotide in the cornea and sclera after short application times (30 min) will also be investigated using fluorescence microscopy. All collected data will be then compared with the literature and referred to *in vivo* and *in vitro* permeation experiments through human and animal ocular barriers. The availability of this permeability data can be of great help for the development of accurate pharmacokinetic models, an important prescreening tool to estimate the likelihood of obtaining therapeutic concentrations at the target site.[11]

MATERIALS AND METHODS

Materials

4-(2-Hydroxyethyl)-1-piperazineethanesulfonic acid (HEPES) was purchased from Sigma–Aldrich (St. Louis, Missouri), as well as bovine serum albumin (BSA), fluorescein isothiocyanate conjugate (FITC-BSA, MW 66 kDa), fluorescently labeled dextrans (FD-4, MW 4 kDa; FD-40, MW 39 kDa), cytochrome C (CYTC, MW 12.4 kDa), and melanin from *Sepia officinalis* [Query:PE-Q1 to ALL] AU: 4-(2-Hydroxyethyl)-1-piperazineethanesulfonic ... Sepia officinalis. Please check the sentence for correctness.. A 24-mer single-stranded DNA (OLIGO, 5′-dAdCdC dTdGdG dGdAdC dAdTdC dGdTdT dCdCdA dTdTdC dAdTdA-

3′, MW 7287.8 Da) synthesized and labeled at the 5′ end with fluorescein at the Centre for Drug Research, University of Helsinki (Helsinki, Finland). Avastin® (Roche Pharma, Reinach, Switzerland) [Query:PE-Q1 to ALL] AU: Please check the updated location information of Roche Pharma for correctness. was used as a source of bevacizumab (BEVA, MW 149 a). Composition: 25 mg/mL bevacizumab; 60 mg/mL α,α-trehalose dihydrate; 0.4 mg/mL polysorbate 20; 5.8 mg/mL sodium phosphate monobasic monohydrate; 1.2 mg/mL sodium phosphate dibasic anhydrous (pH 6.2).[12] Bevacizumab derivatization FITC conjugation occurs through the free amino groups of bevacizumab, forming a stable thiourea bond.[13] The derivatization procedure was explained in detail in a previous paper.[14] Briefly, 250 μL of a FITC solution (1 mg/mL) in 0.1 M carbonate/bicarbonate buffer (pH 9) were added to 1 mL of bevacizumab (5 mg/mL) in 0.1 M carbonate/bicarbonate buffer. The mixture was incubated at 20 ± 2°C for 2 h protected from light. Then, the labeled bevacizumab was separated from the free FITC on a Sephadex G-25M column (Sigma–Aldrich). The concentration of bevacizumab [$\text{Beva}_{(\text{mg/mL})}$] after conjugation was determined by measuring the absorbance at 280 nm (A_{280}), assuming that the extinction coefficient ($E_{280}^{0.1\%}$ = 1.4) was not altered by conjugation[15] and taking into account the correction factor because of the absorbance of FITC at [Query:PE-Q1 to ALL] We have moved the ref citation 15 here from equation 1. Please check for correctness. 280 nm (0.35 × A_{495})[15, 16]:

$$\text{Beva}_{(\text{mg/mL})} = \frac{A_{28} - (0.35 \times A_{495})}{E_{280}^{0.1\%}} \tag{1}$$

Buffer solutions were HEPES−buffered saline (5.96 g/L HEPES, 9.0 g/L NaCl pH 7.4 with NaOH 5 N) and phosphate−buffered saline (PBS; 0.19 g/L KH_2PO_4, 5.98 g/L Na_2HPO_4•$12H_2O$, 8.8 g/L NaCl pH 7.4 with H_3PO_4). All the other chemicals used were of analytical grade.

Tissue Preparation

Fresh porcine eyes were isolated from Landrace e Large White (age 10–11 months, weight 145–190 kg, both female and male animals) and were supplied from a local slaughterhouse (Annoni S.p.A., Parma, I). The eyes were kept in PBS at ±4°C until the dissection carried out within 2 h from the enucleation. In the first step, muscular and connective tissues around the eye-bulb were completely removed. The isolation of the cornea was described in a previous paper.[17] Briefly, the full-thickness cornea (epithelium, stroma, and endothelium, C-FULL), was isolated as a corneo-scleral button-shaped piece, cutting with a scalpel beyond the limbus of bulbs with macroscopically intact cornea. To obtain de-epithelialized cornea (C-DEP), the whole eye bulb was soaked in deionized water at

60°C for 2 min to remove the epithelium. In order to avoid tissue damage during the preparation, corneal tissues were exposed to air only for a few minutes and once prepared, all samples were kept into an isotonic solution (0.9% NaCl) until their use that took place within 30 min. In the isolation of the CH-BM, starting from a whole eye bulb, the anterior segment was removed, then vitreous and retina were discarded and the choroid-Bruch's layer was carefully removed from sclera; both pigmented (containing melanin) and nonpigmented samples (no melanin) were isolated. Following the same method, the sclera (SC) and the sclera-choroid-Bruch's layer (S-CH-BM) were isolated. Only the equatorial part of the sclera (thickness: 1.25 ± 0.25 mm) was used for the permeation experiments.

Permeation Experiments

Permeation experiments were performed in glass Franz-type diffusion cells (Disa, Milan, Italy). In the case of cornea and CH-BM samples, the diffusion area was 0.2 cm^2, and in the case of the sclera and the trilayer, the diffusion area was 0.6 cm^2. The donor compartment (volume 1 mL) was filled with 300 μL of solution containing the macromolecule in HEPES buffer, except for bevacizumab, when PBS buffer was used. Concentrations and experimental conditions are summarized in Table 1. Different donor concentrations were linked to the diverse sensitivity of analytical methods used and to the different permeability of the tissues under investigation. In the case of FITC-bevacizumab, the postderivatization concentration of 2.5 mg/mL was used in all cases. The receiving phase consisted of 4 mL of HEPES buffer (PBS in the case of bevacizumab) thermostated at 37°C and stirred with a magnetic bar. At predetermined times, samples of 300 μL were taken from the receiving compartment and immediately replaced by an equal volume of fresh buffer. Permeation was followed for 5 h, unless otherwise indicated. All samples containing fluorescent probes were carefully protected from light using aluminum foil until analysis.

Table 1 [Query:PE-Q1 to ALL] AU: Please check the presentation of Tables 1 and 2 for correctness. **Characteristics of the Model Molecules Used, Experimental Conditions, and Apparent Permeability Coefficient (Average ± SD)**

	Experimental Conditions	Results				
Compound	MW (kDa)	Stoke's Radius (Å)	Charge (pH 7.4)	Tissue	Donor Concentration (mg/mL)	P_{app} × 10^6 (cm/s)
Dextran (FD-4)	4.4[a]	14[a]	Neutral ζ: ~2.68 ± 0.56 mV[18, 19]	C-FULL	1	0

				C-DEP	1	1.70 ± 0.86
				CH-BM	0.1	12.13 ± 10.04[b]
				SC	0.1	1.08 ± 0.28
24-mer ssDNA (OLIGO)	8	20	Negative	C-FULL	1.5	0
				C-DEP	1.5	1.89 ± 0.95
				CH-BM pigmented	0.025	5.3 ± 5.02[c]
				CH-BM not pigmented	0.025	27.5 ± 5.6[c]
				SC	0.25	1.32 ± 0.87
				S-CH-BM	0.25	0.41 ± 0.18[b]
Cytochrome C (CYT C)	12.4	17.8–20.1[20]	Positive (+9 at pH 8)	C-FULL	70	0
				C-DEP	70	3.17 ± 0.71
				CH-BM	0.5[21]	13.5[d][21]
				SC	10[21]	2.16 ± 0.49[21]
Dextran (FD-40)	39[a]	45[a]	Neutral ζ: −2.68 ± 0.56 mV[18, 19]	C-FULL	2	0
				C-DEP	2	0.097 ± 0.083
				CH-BM	0.5	6.82 ± 3.42[b]
				SC	0.5[22]	0.27 ± 0.11[22]
Bovine serum albumin (FITC-BSA)	67	36	Negative ζ: −23 mV[23]	C-FULL	2	0
				C-DEP	2	0.77 ± 0.04

				CH-BM	0.1	11.7 ± 2.2[b]
				SC	2	0.18 ± 0.12
Bevacizumab (FITC-BEVA)	149	55	Neutral ζ: −3.32 ± 0.87 mV[14]	C-FULL	2.5	0
				C-DEP	2.5	0
				CH-BM pigmented	2.5	3.47 ± 0.82[b]
				SC	2.5	0.05 ± 0.07 µg[e]

[a]From suppliers.

[b]Average of pigmented and not pigmented ($p > 0.05$).

[c]Experiment time 2 h.

[d]Differences in lag-time: 80 min for pigmented, whereas no lag-time for not pigmented.

[e]Amount permeated after 5 h. Permeability coefficient is not calculable as the steady state was not reached.
C-FULL, full-thickness cornea (epithelium, stroma, and endothelium); C-DEP, de-epithelialized cornea; CH-BM, choroid-Bruch's membrane bilayer; SC, sclera; S-CH-BM, sclera-choroid-Bruch's membrane trilayer.

All the conditions were tested three to four times, with the exception of oligonucleotide permeation across the sclera ($n = 13$) and across S-CH-BM ($n = 8$).

Analytical Methods

All fluorescent permeants were analyzed without any preliminary separation with fluorescence multilabel plate reader (Viktor^3 1420; Wallac or Cary Eclipse, Varian; λ_{ex} 485 nm, λ_{em} 535 nm). Cytochrome C was analyzed with a HPLC/UV system (Flexar, Perkin-Elmer, Norwalk, Connecticut) with a 150 × 4.6 mm^2 column packed with 5 µm C18 silica reversed-phase particles (Phenomenex, LePecq, France) and equipped with a security guard column (Security Widepore). The mobile phase A (aqueous) was 0.1% TFA (trifluoroacetic acid) in a mixture of distilled water and CH_3CN (95:5 vol %), whereas the phase B (organic) was 0.1% TFA in CH_3CN. The flow rate was 1.6 mL/min. The LC gradient program [time (min)/% mobile phase B] was set to 0.01/25, 6/55, 9/55, 9.1/25, and 12/25. Temperature was kept at 40°C and the absorption was monitored at 214 nm. The injection volume was 100 µL. The retention time of cytochrome C was approximately 4 min. Linearity was obtained in the concentration range of 5–500 µg/mL; RSD% (relative standard deviation%) and ER% (relative error%) were lower than 15%. The LOD (limit of detection) and the LLOQ (lower limit of

quantification) were 2.5 and 5 μg/mL, respectively.

Fluorescence Microscopy

In order to evaluate the distribution of macromolecules inside the tissues after 30 min of permeation experiments, porcine cornea and sclera were frozen in liquid nitrogen. The samples were then immersed in Killik frozen section medium (Bio-Optica, Milan, Italy) and sectioned in 8-μm thick slices with a rotary cryomicrotome (Reichert-Jung Frigocut 2700, Nussloch, Germany). Sections were rinsed in PBS, mounted on polylysine precoated microscope slide and covered with the coverslips, previously coated with a fluorescence mounting medium (PBS:glycerol = 50:50). Tissues were analyzed with an optical microscope equipped with a fluorescence filter Nikon Eclipse 80i (λ_{ex} 465 nm; λ_{em} 495 nm). Images were taken with a Nikon Digital Sight DS-2mV camera (Nikon Instruments, Calenzano, Italy) using NIS Elements F software (Nikon Instruments) and analyzed with ImageJ Software.[24]

Data Processing

Permeated amount (μg/cm^2) is presented as a function of time (min). The transmembrane flux of macromolecules (J, μg/cm^2 min) is calculated from the slope of the regression line at steady state, and the apparent permeability coefficient (P_{app}, cm/s) is calculated at the steady state as:

$$P_{\mathrm{app}} = J/C_{\mathrm{D}} \tag{2}$$

where C_D (μg/mL) is the concentration of the donor solution. The lag−time (min) was determined from the intercept on the x−axis of the regression line at steady state. Blank experiments were conducted to exclude the presence of any interference from the tissue.

Statistical Analysis

Results in Tables 1 and 2 are expressed as mean value ± SD. For the sake of clarity, in the figures, the standard error of the mean (SEM) is reported instead of SD.

Table 2 Trans-Scleral Permeability Coefficient of Macromolecules

Proteins						
Molecules Tested	MW (kDa)	Radius (Å)[a]	P × 10^6 (cm/s)	Sclera[b]	Sclera Thickness (μm)	Reference
Insulin	5.7	11.3–20	1.93 ± 0.32	H	590	25

Insulin	5.7	11.3–20	0.85 ± 0.48	P	1250	25
Cytochrome C	12.4	20	2.16 ± 0.49	P	1250	21
Basic fibroblast growth factor	16	30	0.012 ± 0.0077	H	–	26
Fluorescein–ovalbumin	45	30.5	0.77	P	810	27
Ranibizumab	48	42	0.85[c]	H	600–1000	28
HSA	69	34	0.06–0.15	B	1000	29
FITC-BSA	70	36	2.38 ± 0.45	H	600 ± 49	30
FITC-BSA	70	36	0.83 ± 0.5	H	810 ± 280	31
BSA	68	36	4.0[c]	H	–	32
FITC-BSA	66	54	0.90 ± 0.50	H	600–1000	28
FITC-BSA	70	33	4.15	P	850[d]	19
FITC-BSA	67	36	0.18 ± 0.12	P	1250	This work
FITC-BSA	67	36	5.49 ± 2.12	R	416 ± 21	33
FITC-BSA	67	36	6.8	R	–	34
Hemoglobin	65	27	0.11–0.47	B	1000	29
FITC-IgG	150	55	4.61 ± 2.17	R	416 ± 21	33
FITC-bevacizumab	149	55	0.53 ± 0.73	H	600 ± 70	14
Bevacizumab	149	55	0.8[c]	H	–	32
Bevacizumab	149	63	0.29 ± 0.14	H	600–1000	28
FITC-bevacizumab	149	63	0.05 ± 0.07 μg[e]	P	1250	This work
Single-Stranded Oligonucleotides						
Molecules Tested	MW (kDa)	Radius (Å)[a]	P×10^6 (cm/s)	Sclera[b]	Sclera Thickness (μm)	Reference
Fluorescein-12-mer	4	–	0.09 ± 0.02	B	–	9
Fluorescein-12-mer	4	–	0.75	B	–	35
Fluorescein-24-mer	8	–	0.77 ± 0.18	H	–	36
Fluorescein-24-mer	8	–	1.32 ± 0.87	P	1250	This work
Fluorescein-24-mer	8	–	0.19 ± 0.01	B	–	9
Fluorescein-24-mer	8	–	0.85	B	–	35
Fluorescein-36-mer	12	–	0.17 ± 0.05	B	–	9
Fluorescein-36-mer	12	–	0.63	B	–	35
Other Macromolecules						

Molecules Tested	MW (kDa)	Radius (Å)[a]	P × 10^6 (cm/s)	Sclera[b]	Sclera Thickness (μm)	Reference
Inulin	5	14	9.0 ± 2.2	H	610 ± 90	37
Inulin	5	14	1.0–1.97	B	1000	29
Inulin	5	14	2.54 ± 0.35	R	-	38
FITC-dextran 4000	4	14	8.87[c]	H	–	32
FITC-dextran 4000	4.4	14	2.67 ± 0.07	P	1250	39
FITC-dextran 4000	4.4	14	1.08 ± 0.28	P	1250	This work
FITC-dextran 4000	4.3	14	0.71 ± 0.09	B	–	9
FITC-dextran 4000	4.4	14	25.2 ± 5.1	R	416 ± 21	33
Radiolabeled dextran 10000	10	23	6.4 ± 1.7	H	610 ± 90	37
Rhodamine-dextran 10000	10	–	1.5	H	–	40

Table 2 continued.

Proteins						
Molecules Tested	MW (kDa)	Radius (Å)[a]	P × 10^6 (cm/s)	Sclera[b]	Sclera Thickness (μm)	Reference
FITC-dextran 10000	9.5	23	0.38 ± 0.06	B	–	9
FITC-dextran 10000	10	23	0.5	B	–	41
Fluorescein-dextran 10000	10	23	4.5 ± 2.2	R	440 ± 90	42
Tetramethylrhodamine-dextran 10000	10	30	0.7 ± 0.35	H	–	26
FITC-dextran 20000	20.0	32	2.25[c]	H	–	32
FITC-dextran 20000	20	52	0.34[c]	H	600–1000	28
FITC-dextran 20000	20.2	32	0.38 ± 0.18	B	–	9
FITC-dextran 20000	16.9	32	6.79 ± 4.18	R	416 ± 21	33
Radiolabeled dextran 40000	40	45	4.9 ± 2.4	H	610 ± 90	37
Rhodamine-dextran 40000	40	–	0.7	H	–	40
FITC-dextran 40000	40	66	0.32[c]	H	600–1000	28
FITC-dextran 40000	39	45	0.35 ±	P	1250	39

			0.12				
Dextran 40000	38	45	0.26	±	B	–	9
			0.04				
FITC-dextran 40000	38.9	45	2.79	±	R	416 ± 21	33
			1.58				
Fluorescein-dextran 40000	40	45	2.2 ± 0.6		R	440 ± 90	42
Polystyrene sulfonic acid	67	69	2.9[c]		H	–	32
Radiolabeled dextran 70000	70	60	1.9 ± 0.4		H	610 ± 90	37
Rhodamine-dextran 70000	70	–	0.4		H	–	40
FITC-dextran 70000	70	60	0.082	±	H	600 ± 49	30
			0.012				
FITC-dextran 70000	70	54	1.86	±	P	850[d]	19
			0.96				
Positive FITC-dextran 70000	70	54	2.44	±	P	850[d]	19
			1.29				
Negative FITC-dextran 70000	70	54	0.79	±	P	850[d]	19
			0.22				
FITC-dextran 70000	77	60	0.10	±	B	–	9
			0.06				
FITC-dextran 70000	71.2	60	1.39	±	R	416 ± 21	33
			0.88				
Fluorescein-dextran 70000	70	60	2.6 ± 1.3		R	440 ± 90	42
Rhodamine dextran 70000	70	60	1.35	±	R	416 ± 21	33
			0.77				
FITC-Ficoll 70000	70	72	1[c]		H	600–1000	28
FITC-Ficoll 70000	70	34	1.37	±	P	850[d]	19
			0.54				
Positive FITC-Ficoll 70000	70	34	0.62	±	P	850[d]	19
			0.27				
Negative FITC-Ficoll 70000	70	34	6.81	±	P	850[d]	19
			2.46				
FITC-dextran 150000	150	85	0.097	±	H	600 ± 49	30
			0.022				
FITC-dextran 150000	120	85	0.48	±	H	590	39
			0.06				
FITC-dextran 150000	150	90	0.8[c]		H	600–1000	28
FITC-dextran 150000	120	85	0.16	±	P	1250	39
			0.07				

FITC-dextran 150000	150	85	1.34 ± 0.88	R	416 ± 21	[33]

[a]Discrepancy among the values of the same macromolecule can be ascribed to different determination methods.

[b]H, human; P, porcine; B, bovine; R, rabbit.

[c]Approximative value estimated/calculated from figures and experimental details.

[d]Average value, calculated from permeability coefficient and diffusion coefficient as reported in the reference paper.

[e]Amount permeated after 5 h. Permeability coefficient is not calculable as the steady state was not reached.

The difference between values was assessed using either one-way ANOVA (Kaleidagraph 4.01 software) followed by Bonferroni test or Student's *t*-test and considered statistically significant when $p < 0.05$.

RESULTS AND DISCUSSION

The properties of a macromolecular drug depend upon its structure and MW. These factors influence molecular radius, shape, and isoelectric point that, in turn, can impact on the interaction with extracellular matrix and connective fibers constituting the tissues. In the end, these properties can influence their partition, accumulation, and permeation characteristics and thus their bioavailability after ocular application. In this paper, six macromolecules are investigated: an oligonucleotide, two proteins, an antibody, and two high MW neutral dextrans, providing a variety of physicochemical properties. The characteristics of the molecules selected are reported in Table 1. The molecular radius reported is the hydrodynamic (or Stoke's) radius that equals to the radius of a sphere diffusing at the same rate in an aqueous solution. Stoke's radius is appropriate in the case of globular proteins (albumin, cytochrome, and bevacizumab), whereas in the case of oligonucleotides or dextrans, it is less pertinent, as they have a more flexible structure and a higher deformability.[18] Oligonucleotides probably have a worm-like structures and dextrans are random coil extended polymers with asymmetric configurations. Both molecules can change their conformation and diffusivity with the ionic strength and concentration.[43, 44] Finally, dextrans and bevacizumab are neutral molecule, whereas oligonucleotides and cytochrome are examples of negatively and positively charged macromolecules.

Table 1 shows the relevant permeation parameters obtained in this work.

Trans-Scleral Permeability

There are several static and dynamic barriers to trans-scleral administration. Figure 2 represents schematically the static barriers to the permeation. The dynamic barriers will be described in *Other*

Barriers to the Posterior Eye Segment. The outermost barrier that a drug has to cross is the sclera. The diffusion of macromolecules across the sclera has been previously reviewed[6, 45] but a comprehensive report of permeability data is still lacking. Here, we present Table 2 where, as far as we know, the existing permeation data of oligonucleotides, proteins, dextrans, and other macromolecules such as ficolls, polystyrene sulfonic acid, and inulin have been collected. This data is also shown in Figure 3 as a function of the MW (Fig. 3a) and molecular radius (Fig. 3b). Apparently, as also reported by other authors, the Stoke's radius is a better predictor of the permeability than the MW, although the correlation between the permeability and molecular radius is still very poor. Only a slight decreasing trend can be seen and the data variability is very large. The source of variability can lie both in the source of sclera and in the characteristics of the macromolecules that, although having the same Stoke's radius, can differ in charge, shape, and conformability/flexibility.

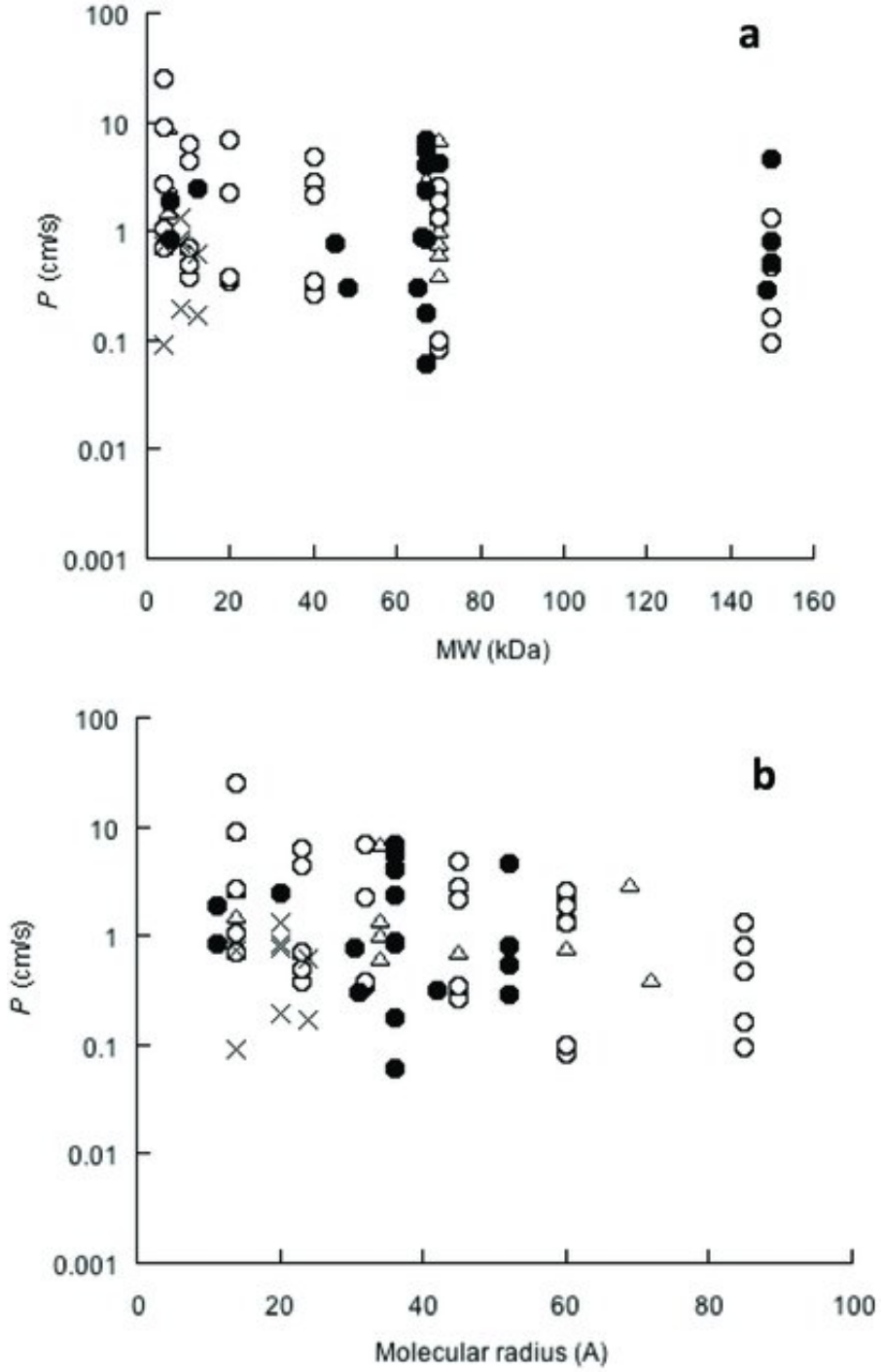

Figure 3 Permeability coefficient of the molecules tested as a function of the MW (a) and molecular radius (b). Proteins are represented by full circles (●), neutral dextrans by open circles (○), oligonucleotides by crosses (Í), and the remaining molecules by open triangles (∆). Permeability coefficient and molecular radius are taken from Table 2. When different radii were reported for the same molecules, the most represented value was used. In case of oligonucleotides, molecular radius of 14 (12-mer), 20 (24-mer), and 24 (36-mer) were used.

To check the role of the sclera thickness, we have collected all the available data for albumin (human and BSA, both FITC conjugated and nonconjugated) and reported it in Figure 4 as a function of the inverse of the sclera thickness. As can be seen, a linear correlation is obtained (R^2 = 0.78), suggesting that differences between animal models can be at least in part because of the different

tissue thickness (rodent/murine < human < porcine < bovine), in agreement with the Fick's law:

$$J = \frac{\mathrm{d}M}{\mathrm{d}t}\frac{1}{A} = \frac{DK}{h}C_{\mathrm{d}}$$
$$P = \frac{DK}{h} \tag{3}$$

where J (μg/cm^2 s) is the trans−scleral flux, dM/dt (μg/s) is the permeation rate, A (cm^2) is the permeation area, C_{d} (μg/mL) is the concentration of the molecule in the donor solution, K is the sclera/vehicle partition coefficient, D (cm^2/s) is the diffusion coefficient, and h (cm) is the diffusion path length.

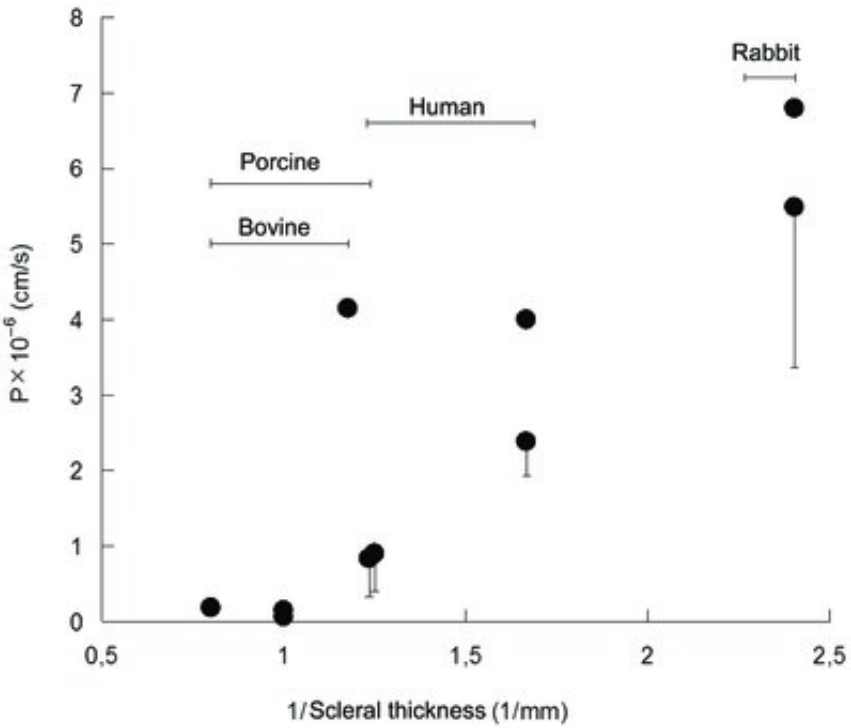

Figure 4 Permeability coefficient of albumin across the sclera as a function of the inverse of the scleral thickness; data are taken from Table 2. When the sclera thickness was not reported, a thickness of 400 μm (rabbit), 600 μm (human), and 1250 μm (porcine and bovine) was used for the calculation.

Yet, also after thickness normalization (i.e., calculation of *DK*), still a 20-fold difference in the permeability coefficient of albumin exists. This could be attributed to differences in the organization of collagen fibers that impact on its tortuosity and thus on the diffusion path length. Because the porosity of sclera is rather high, its thickness matches rather well with the diffusion path length of small solutes, whereas macromolecules cannot pass all the smallest pores but have to find a tortuous path for penetration. Finally, it is important to notice that the duration of an experiment can

also influence the measured permeability coefficient, as demonstrated by Wen et al.[46] using small-sized drugs.

Concerning the role of the macromolecular characteristics on the trans-scleral permeability, very little data are available in the literature. To elucidate the role of the molecular radius more closely, only neutral dextrans were selected under study. Dextrans are polysaccarides composed of glucose monomers and have the same structure, zeta potential, and molecular conformation, differing only in their molecular radius. In Figure 5, their permeability versus inverse of radii is shown, in agreement with the Stoke–Einstein equation. Again, the difference between the different animal models is evident, also after the normalization of the tissue thickness.

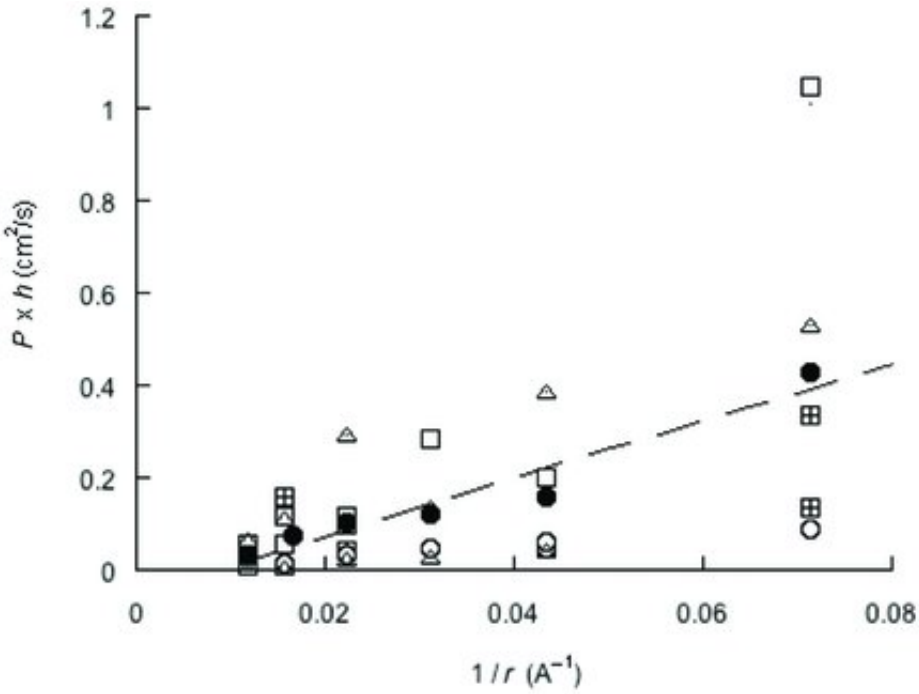

Figure 5 Permeability coefficient of neutral dextrans multiplied by the sclera thickness as a function of the inverse of molecular radius ($1/r$; A^{-1}) (data from Table 2). When the sclera thickness was not reported, a thickness of 400 μm (rabbit), 600 μm (human), and 1250 μm (porcine and bovine) was used for the calculation. Different symbols refer to the different source of sclera used; bovine (open circles, ○), rabbit (open squares, c), porcine (crossed squares), human (open triangle Δ). Full circles (●) indicate the average value.

In addition to the molecular radius, shape, charge, and conformation can also have a role. Recently, Wen et al.[28] compared proteins and dextrans and found that dextrans had a higher normalized permeability across the sclera (permeation coefficient normalized by the aqueous diffusion coefficient) as compared with proteins of comparable MW, probably because of higher structure flexibility, analogously to reports of diffusion of proteins, and polysaccharides across other porous membranes. On the contrary, Srikantha et al.[19] reported slower diffusion of neutral dextran

and neutral Ficoll compared with that of albumin.

Another molecular feature that has an impact on the trans-scleral permeability is the charge. The role of the charge is still controversial even in case of low MW compounds. Some authors suggest that the sclera is more permeable to negatively charged molecules,[29, 47] whereas others report that positively charged molecules partition and cross the sclera more easily.[46, 48] Ranta et al.[9] studied the permeability of oligonucleotides (4–12 kDa) across bovine sclera and found values lower than those obtained with both dextrans and proteins of similar molecular radii. This was explained by the negatively charged polymers such as hyaluronic acid and GAGs in the sclera preventing the partitioning of negatively charged molecules because of charge repulsion.[49, 50] However, in the present paper, the permeation of the oligonucleotide is reasonably in-line with its size, whereas cytochrome C (positively charged) permeation resulted in a significantly higher permeability coefficient (Table 1).

The analysis of the data in Table 2 does not permit to draw conclusions of the effect of the charge on the permeability of macromolecules, also because differences in the charge often follow differences in the shape and conformation. In this regard, Srikantha et al.[19] studied macromolecules diffusion across the sclera using neutral, cationic, and anionic Ficoll and dextrans with MW of 70 kDa. Their results indicate that a charge have a different impact on the permeability, depending on the structure of the molecules, suggesting that a charge can have an indirect effect because of a change in the molecular conformation. Another reason that makes the evaluation of the role of the charge on the permeability difficult is that, because of ion binding, the charge number of a macromolecule in the solution is different from that calculated from its p*K*a value. For example, the charge number of cytochrome C at pH 8.25 and in 0.15 M NaCl has been measured to be as low as +1.4[51] and that of BSA −2.3 (0.01 M NaCl, pH 6.4–6.8).[52] Hence, the comparison of data from various sources is rather difficult.

Finally, both negative and positive compounds can interact with the sclera. Drug adsorption on connective tissues has been demonstrated with streaming potential measurements using molecules of different charge and MW.[53, 54] Also, neutral molecules could in principle interact with the sclera via nonionic interactions and specific binding sites: it has been found, for instance, that sclera contains binding sites for insulin and for insulin-like growth factor-1.[55] Additionally, recent data suggest that more than the net charge of a protein, its electrostatic potential distribution (and in particular the presence/absence of regions of high and low charge distribution as well as the presence of hydrophobic regions) is responsible for the interaction with the transport pathway.[56] It is also

important to underline that scleral binding can have different effect on drug delivery: on one hand, it can hinder drug diffusion, on the other hand, it can create a drug reservoir into the tissue that permits to obtain a sustained release, as demonstrated with both high[22] and low[57] MW compounds.

Permeability Across the CH-BM

The choroid is a vascular layer composed of capillaries and supported by the Bruch's membrane, a connective membrane of 2–4 μm thickness, forming the main barrier to permeation across the choroid-Bruch's bilayer.[58-60] Permeability data of macromolecules in this layer is very scarce and, until now, has merely been performed to evaluate the translocation of nutrients and waste products across the Bruch's membrane. Yet, the permeability found is relatively high. Human serum proteins (MW 39–211 kDa) are able to cross human choroid-Bruch's layer *in vitro*,[61] as well as FITC–dextrans (MW 4.4–500 kDa)[58] or even fluorescently labeled low-density lipoproteins (MW: 2400–3900 kDa; size 19–23 nm).[62] The permeability data obtained in this work (Table 1) highlight that no trend regarding the charge or size is observable. Only bevacizumab shows a significantly lower permeation, probably as a consequence of the much higher MW and radius.

In addition to the barrier properties of the Bruch's membrane, also the presence of melanin should be considered. In fact, the amount of melanin is quite high in the choroid and it is known to bind several drugs, hampering their transport to the retina.[63] This has an effect on both the permeability coefficient and/or on the lag time. In the literature, very little data of the interaction between macromolecules such as proteins and gene materials and melanin is available. Pitkänen et al.[64] found that 21-mer or 10-mer phosphodiester oligonucleotides did not bind either synthetic melanin or melanin isolated from bovine eyes. On the contrary, the affinity of cytochrome C to porcine melanin inside the choroid was demonstrated by *in vitro* binding studies and confirmed by permeation experiments.[21]

In the present work, an attempt to perform binding studies with isolated melanin from *Sepia officinalis* and 24-mer oligonucleotide, albumin, and bevacizumab was carried out, but because of analytical interferences, conclusions could not be drawn [Query:PE-Q1 to ALL] AU: In the present ... drawn. Please check the sentence for the correctness of the changes made.. However, appreciable results were obtained with the permeation experiments performed through pigmented and not-pigmented isolated CH-BM. In the case of BSA and bevacizumab, the presence of melanin in the tissue did not change the permeability coefficient (Table 1), whereas in case of oligonucleotide, the flux across the nonpigmented tissue was higher than that of the pigmented tissue (Fig. 6), suggesting an interaction of the oligonucleotide

with melanin or melanosomes. The calculated permeability coefficients (Table 1) also show a statistical difference ($p = 0.003$).

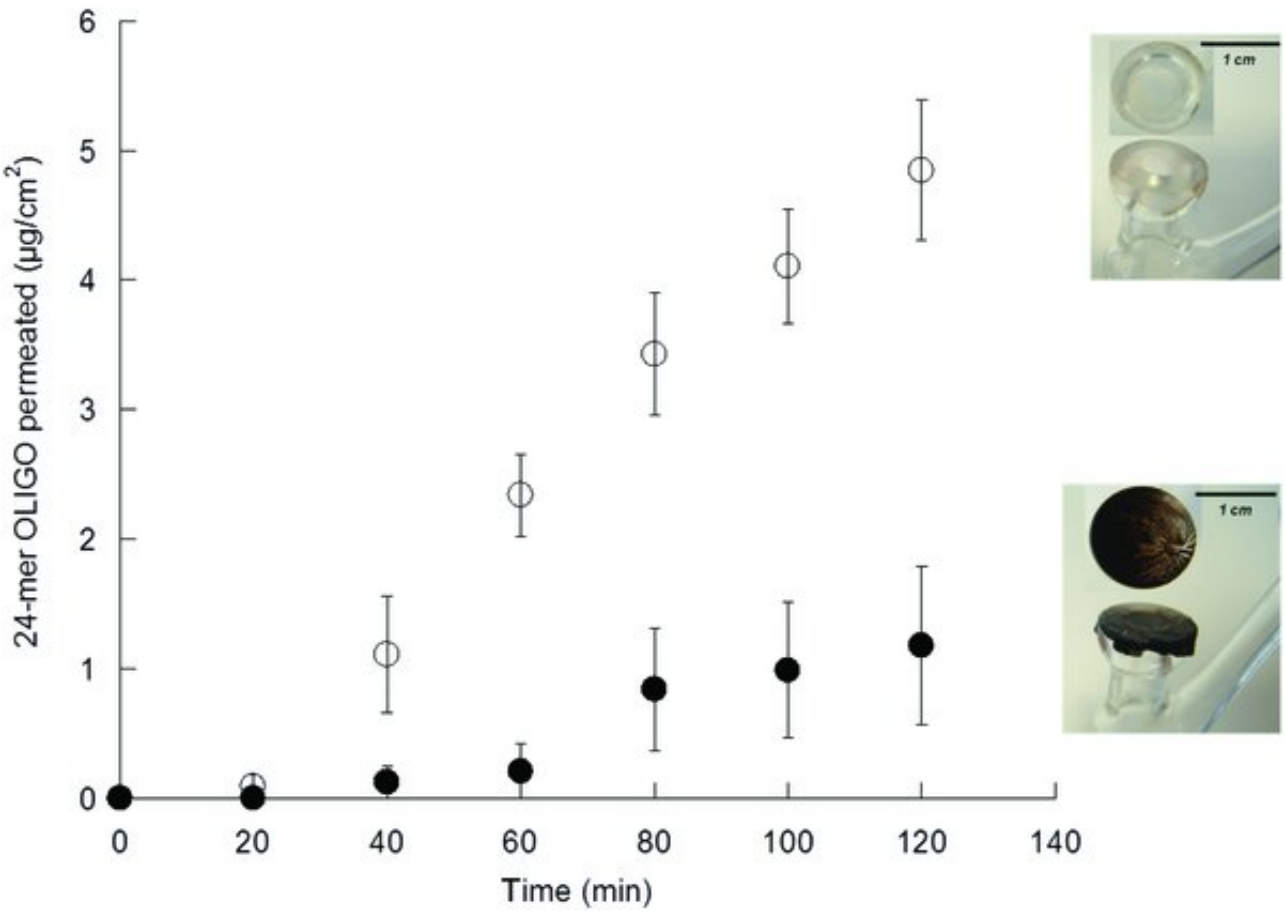

Figure 6 Permeation profiles of 24-mer oligonucleotide across pigmented (full circle, $n = 3$) and not pigmented (void circle, $n = 4$) choroid-Bruch's membrane. The donor concentration was 25 μg/mL. Data are reported as mean ± SEM. The pictures illustrate the choroid-Bruch's membrane with and without melanin mounted on the inferior chamber of a vertical diffusion cell (on the top of each image, vertical view). (Pictures are taken from supplementary data of Pescina et al.[65] with permission from …)[Query:PE-Q1 to ALL] AU: Please provide the name of the publisher of Ref. 81 in the '...' in the caption of Figure 6.].

Despite the relatively high permeability of choroid and despite its thinness, it is interesting to note that the permeability of the oligonucleotide across the trilayer (S-CH-BM) is significantly lower ($p < 0.05$) than that across the isolated sclera (Fig. 7). The calculation of the permeability of the membrane by summing the resistivities ($1/P_{trilayer} = 1/P_{sclera} + 1/P_{CH\text{-}BM}$) results in discrepancy with the values measured directly for the multilayer, $(0.35 \pm 0.06) \times 10^{-6}$ cm/s being the experimental value (with pigmented choroid; Fig. 7) and 1.05×10^{-6} cm/s the calculated value (with pigmented choroid, data from Table 1). This discrepancy could be attributed to the fact that a trilayer takes longer time to reach the steady state.

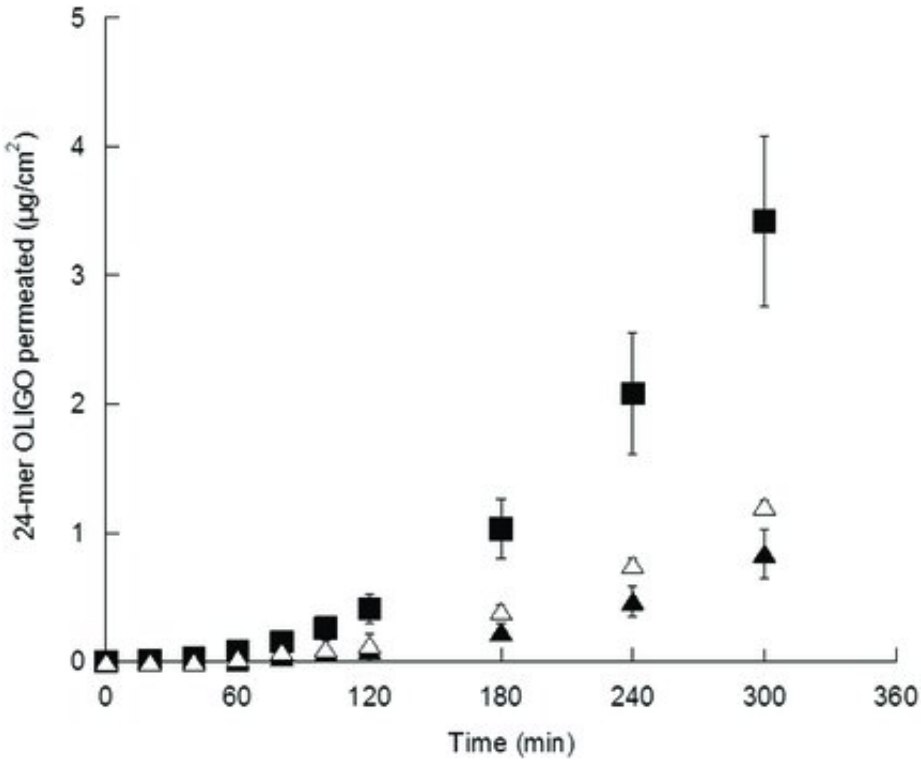

Figure 7 Permeations profiles of a 24-mer ssDNA through porcine sclera (full square, *n* = 13), trilayer having pigmented choroid (full triangle, *n* = 8), trilayer having not pigmented choroid (void triangle, *n* = 4). In all cases, donor concentration was 250 µg/mL and permeation area corresponded to 0.6 cm^2. Data are reported as mean ± SEM.

Permeability Across the Cornea

As expected, none of the macromolecules tested was able to cross the full-thickness cornea in 5 h. The low permeability of corneal epithelium is because of tight junctions that restrict drug diffusion through the paracellular pathway (cut-off 10 Å[6]), limiting the permeation of high MW hydrophilic compounds. Experimental data were corroborated with fluorescence microscopy images shown in Figure 8 and referred to diffusion for 30 min of fluorescently labeled oligonucleotide or bevacizumab in porcine full-thickness cornea (Figs. 8a and 8d), de-epithelialized cornea (Figs. 8b and 8e), and sclera (Figs. 8c and 8f). Because of the high MW and hydrophilicity, both the oligonucleotide and bevacizumab were completely retained by the outer layers of the corneal epithelium, as clearly shown in the fluorescence microscopy (Figs. 8a and 8d).

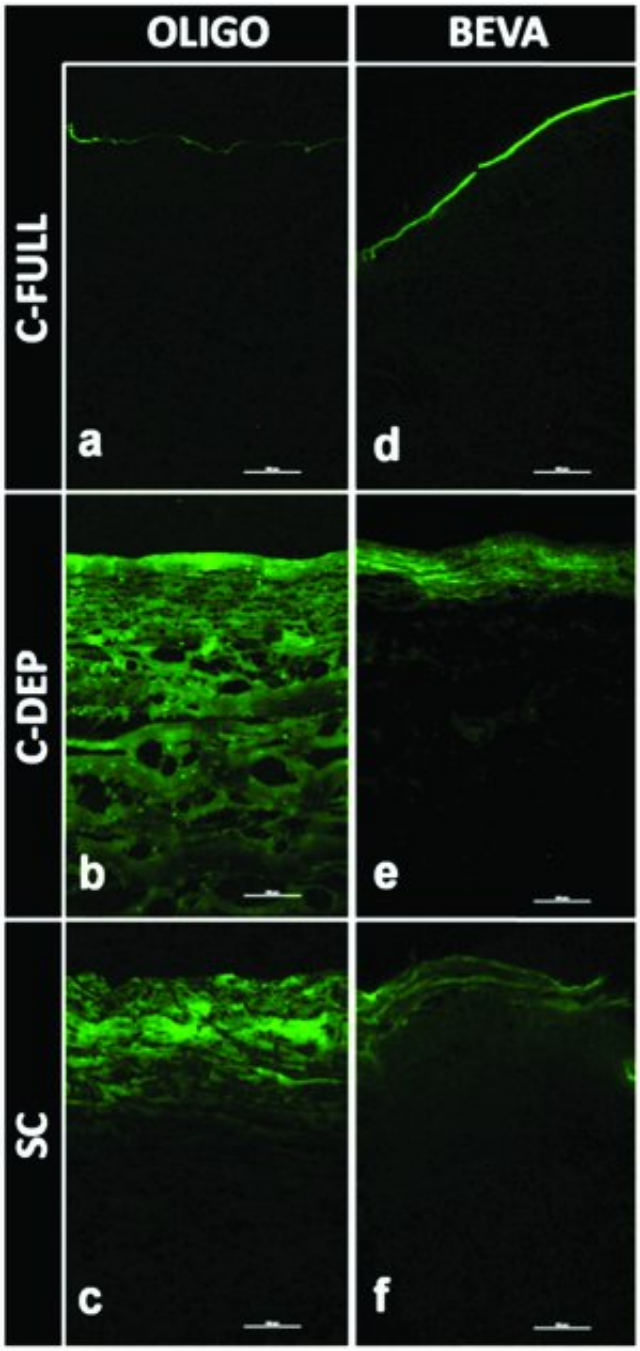

Figure 8 Fluorescence microscopy after 30 min of permeation through full-thickness (upper panels) and de-epithelialized (middle panels) porcine cornea and equatorial region of porcine sclera (bottom panels). Images are referred to oligonucleotide (a–c) and bevacizumab (d–f). (Scale bar, 100 μm).

However, macromolecules and even antibodies are administered topically to treat corneal neovascularisation or other corneal diseases efficiently. For example, bevacizumab for corneal neovascularisation,[66] infliximab for ocular surface scarring,[67] and antisense oligonucleotide for the prevention of cornea graft rejection[68] can be mentioned. The reason for their efficacy is linked to the increased permeability of the corneal epithelium induced by the diseases or by corneal transplant, favoring drug diffusion to the underlying tissues. Therefore, the permeability of the model molecules was also evaluated across de-epithelized cornea, which was chosen as a model of damaged tissue.

The relevant permeability parameters obtained are given in Table 1. An illustrative permeation profile of an oligonucleotide is shown in Figure 9.

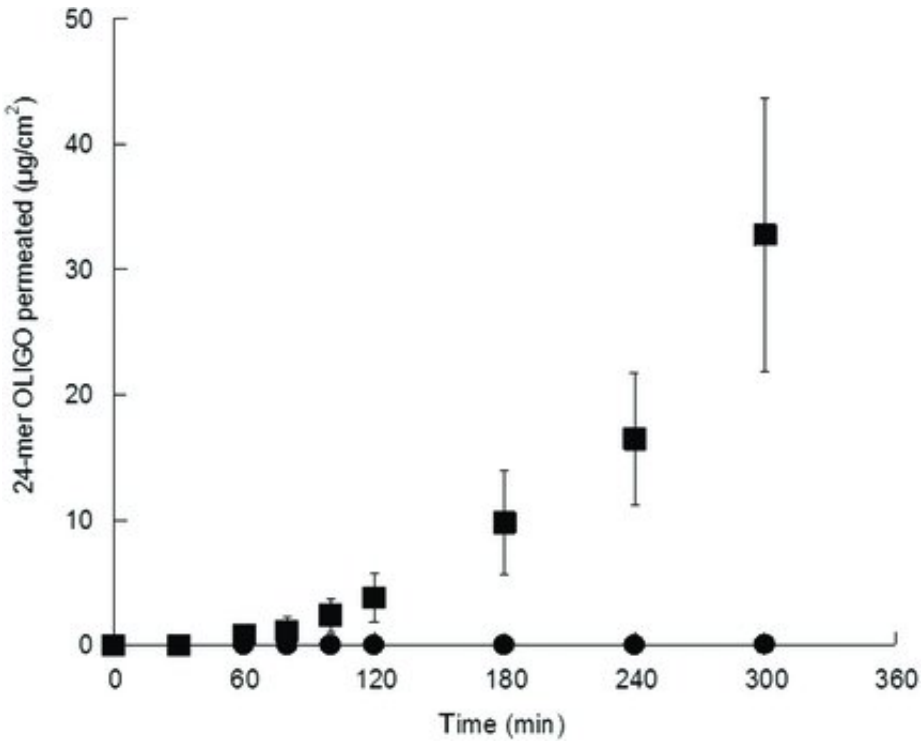

Figure 9 Permeation profiles of 24-mer oligonucleotide across full-thickness (full circle, *n* = 3) and de-epithelialized porcine cornea (full square, *n* = 3), starting from a 1.5-mg/mL donor solution. (Mean ± SEM).

For molecules with a radius equal or lower than 35 Å, the permeability of the bilayer stroma-endothelium is comparable with the permeability of the sclera, in agreement with the literature data for small molecules.[6] Trans-scleral permeation of drugs is comparable to the diffusion into the corresponding stromal water pores.[38] In the case of bevacizumab, on the contrary, substantial differences can be seen between the two tissues. Although no permeation was observed across the de-epitelialized cornea in 5 h, trans-scleral permeation was observed, although the sclera was thicker than the de-epitelialized cornea (~1.2 mm vs. 0.8 mm).

Permeation data were confirmed by fluorescence microscopy. As shown in Figure 8, the diffusion of oligonucleotide was hindered neither by corneal stroma (Fig. 8b), nor by sclera (Fig. 8c). Although the permeability coefficients through the two tissues are similar (Table 1), a deeper fluorescent front is seen in stroma than in sclera.

The fluorescent images taken after 30 min of permeation of bevacizumab confirm its different diffusion rate in the two tissues (Figs. 8e and 8f): depths of bevacizumab diffusion front, measured with ImageJ Software, were 64.4 ± 10 and 151.4 ± 15 µm, for stroma and sclera, respectively. This difference can be related to the different tissue structure. It is known that stroma and sclera have a

similar composition in terms of water content and collagen type but different fibrils diameter and arrangement[69] that can lead to different tissue porosity. We can hypothesize that the different porosity between sclera and corneal stroma do not influence the permeability of molecules with a radius up to 45 Å, but can have an impact on antibodies permeation (radius: 65 Å).

Our data are in agreement with *in vivo* experiments in which bevacizumab, topically applied on intact cornea of healthy mice, was not able to reach the stroma even after 7 days of treatment.[66] In the case of complete epithelium removal, bevacizumab crossed the whole thickness of the stroma in 6 h.[66] Finally, using a mouse model of corneal neovascularisation, because of the inflammation and the loss of integrity, IgG was detectable in stroma after 48 h from the beginning of the application.[66] Another *in vivo* data supporting substantial lack of penetration across intact cornea was reported by Berdugo et al.[70]: a fluorescent 15-mer ODN (MW 5.2 kDa) applied *in vivo* on the rat cornea was not able to entirely cross the tissue and was detectable only into the outermost epithelial layers.

In vitro data on the permeability of macromolecules across the cornea are not abundant and are often conflicting. In general, discrepancies in the permeability of these molecules in the cornea can be attributed to the different source of the tissue (human, porcine, rabbit) and different experimental conditions, such as the duration of permeation experiments, the concentration of the permeant in the donor solution, and the sensitivity of the analytical method.

The diffusion of single-chain variable fragments (scFv) was studied *in vitro* through full-thickness porcine cornea. All permeants were detected into receiving chamber after 7 h, and the same result was observed with a 48-kDa Fab.[71] Similar results were obtained with ESBA105 (both native and fluorescently labeled), a 26.3-kDa scFv antibody having anti-TNF-α activity, across intact rabbit cornea,[72] and with a scFv (28 kDa) and a miniantibody (67 kDa) across porcine cornea.[73] The ability to cross the full-thickness human cornea was recently demonstrated for myoglobin (16.7 kDa) and BSA (66 kDa).[74] On the contrary, even in 10 h, IgG antibodies did not penetrate porcine full-thickness cornea[71] or de-epithelialized cornea.[73] Concerning linear dextrans, different authors have demonstrated passive diffusion of FD-4 through rabbit full-thickness cornea *in vitro* with the permeability coefficient of 0.4×10^{-7}[75] and 0.25×10^{-8} cm/s.[76] FD-4 permeation was significantly increased with chemical enhancers.[75]

Other Barriers to the Posterior Eye Segment

It is important to underline that beyond the static barriers studied in this paper, dynamic barriers are also present *in vivo* and can hinder drug transport to the target. In the case of the treatment of

anterior segment diseases, it seems that the main clearance mechanism (beyond lacrimation and spillage) is represented by the conjunctival blood and lymphatic flows.

When the posterior segment is the target of the therapy, the choroidal circulation can be an important obstacle. In fact, once the drug has crossed the sclera, it can in principle enter the fenestrated capillaries of the choroidal circulation and be removed. However, this mechanism should impact less on macromolecules than on small drugs. In fact, the fenestrations (80–100 nm) present in the choroidal capillaries are covered (shelted/overlied) by radially oriented fibers[77] that reduce the size of the gap and probably limit the clearance of macromolecules.[9, 78] Similarly, Kim et al.[79] showed that although dynamic clearance mechanisms significantly reduced the subconjunctival concentration of a small drug (half-life: 22 min), the clearance rate for albumin was much slower (half-life: 5.3 h) and was comparable in *in vivo* and postmortem experiments. This suggests that dynamic barriers have a limited effect on the ocular clearance of large molecules.

Also, the retinal pigment epithelium, a monolayer of cells anchored on Bruch's membrane and connected with tight junctions, can hinder drug diffusion to the retina. Nonetheless, cultured RPE monolayers are permeable to inulin and horseradish peroxidase (35 kDa)[80] and *ex vivo* bovine RPE-choroid is permeable toward dextran with MW up to 80 kDa.[81] Finally, Amaral et al.[27] demonstrated both *ex vivo* and *in vivo* (on rats) the permeability of PEDF[Query:PE-Q1 to ALL] AU: Please replace PEDF with its full form. and ovalbumin across RPE.

CONCLUSIONS

Macromolecular drugs, such as proteins and oligonucleotides, represent today important therapeutic tools in the treatment of ocular diseases, and the understanding of the molecular basis of the pathologies will further increase the number of possible drug candidate in the next years. As the noninvasive ocular administration of drug is a timely topic, the knowledge and the understanding of macromolecules permeability across ocular barriers is of utmost importance to be able to evaluate the feasibility of a noninvasive administration.

In the present paper, the permeability of macromolecules of different MW, charge, and conformability has been evaluated across different ocular tissues and the results have been completed with an update of literature data. From the data here presented, it is evident that it is difficult to predict macromolecules behavior based on their physicochemical properties, mainly because—opposite to small molecules—there is an interplay among charge, molecular radius, and conformation, that prevent to analyze them separately. However, the information here presented can

be of great help for a rough evaluation of the feasibility of a noninvasive administration to the anterior and posterior segment of the eye and to build computational models in order to improve understanding of the interplay among static, dynamic, and metabolic barriers in the delivery of macromolecules to the eye.

AKNOWLEDGMENTS

The financial support of Italian Ministry of Education, University and Research (PRIN2010H834LS) is gratefully acknowledged. The authors thank Dr. Matteo Goldoni (Department of Clinical and Experimental Medicine, University of Parma) for providing the equipment Cary Eclipse (Varian) and for helpful suggestions.

REFERENCES [Query:PE-Q1 to ALL] AU: References have been renumbered to maintain the journal style of sequential citations. Please check for correctness.

1. National Institutes of Health. 2014. ClinicalTrials.gov. Accessed, at: http://clinicaltrials.gov/. [Query:PE-Q1 to ALL] AU: Please provide the last date (in US format) on which the link in Ref. 1 was last accessed.
2. Kim YC, Chiang B, Wu X, Prausnitz MR. 2014. Ocular delivery of macromolecules. J control Release 190C:172–181.
3. El Sanharawi M, Kowalczuk L, Touchard E, Omri S, de Kozak Y, Behar-Cohen F. 2010. Protein delivery for retinal diseases: From basic considerations to clinical applications. Prog Retin Eye Res 29:443–465.
4. Mohan RR, Rodier JT, Sharma A. 2013. Corneal gene therapy: Basic science and translational perspective. Ocul Surf 11:150–164.
5. Boye SE, Boye SL, Lewin AS, Hauswirth WW. 2013. A comprehensive review of retinal gene therapy. Mol Ther 21:509–519.
6. Prausnitz MR, Noonan JS. 1998. Permeability of cornea, sclera, and conjunctiva: A literature analysis for drug delivery to the eye. J Pharm Sci 87:1479–1488.
7. Ranta VP, Laavola M, Toropainen E, Vellonen KS, Talvitie A, Urtti A. 2003. Ocular pharmacokinetic modeling using corneal absorption and desorption rates from in vitro permeation experiments with cultured corneal epithelial cells. Pharm Res 20:1409–1416.
8. Ranta V-P, Urtti A. 2006. Transscleral drug delivery to the posterior eye: Prospects of pharmacokinetic modeling. Adv Drug Deliv Rev 58:1164–1181.
9. Ranta V-P, Mannermaa E, Lummepuro K, Subrizi A, Laukkanen A, Antopolsky M, Murtomäki L, Hornof M, Urtti A. 2010. Barrier analysis of periocular drug delivery to the posterior segment. J Control Release 148:42–48.
10. Kotha S, Murtomaki L. 2014. Virtual pharmacokinetic model of human eye. Math Biosci 253:11–18.
11. Pepic I, Lovric J, Cetina-Cizmek B, Reichl S, Filipovic-Grcic J. 2014. Toward the practical implementation of eye-related bioavailability prediction models. Drug Discov Today 19:31–44.
12. US FDA (2011). Avastin® (Bevacizumab) final labeling text. Accessed April 2014, at: http://www.accessdata.fda.gov/drugsatfda_docs/label/2011/125085s225lbl.pdf. [Query:PE-Q1 to ALL] AU: Please provide the date on which the link in Ref 12 was last accessed.
13. Wood BT, Thompson SH, Goldstein G. 1965. Fluorescent antibody staining. 3. Preparation of fluorescein-isothiocyanate-labeled antibodies. J Immunol 95:225–229.
14. Pescina S, Ferrari G, Govoni P, Macaluso C, Padula C, Santi P, Nicoli S. 2010. In vitro permeation of

bevacizumab through human sclera: Effect of iontophoresis application. J Pharm Pharmacol 62:1189–1194.

15. McKinney RM, Spillane JT, Pearce GW. 1966. A simple method for determining the labeling efficiency of fluorescein isothiocyanate products. Anal Biochem 14:421–428.

16. Mahler HC, Muller R, Friess W, Delille A, Matheus S. 2005. Induction and analysis of aggregates in a liquid IgG1-antibody formulation. Eur J Pharm Biopharm 59:407–417.

17. Pescina S, Govoni P, Potenza A, Padula C, Santi P, Nicoli S. 2015. Development of a convenient ex vivo model for the study of the transcorneal permeation of drugs: Histological and permeability evaluation. J Pharm Sci 104:63–71.

18. Venturoli D, Rippe B. 2005. Ficoll and dextran vs. globular proteins as probes for testing glomerular permselectivity: Effects of molecular size, shape, charge, and deformability. Am J Physiol Renal Physiol 288:F605–F613.

19. Srikantha N, Mourad F, Suhling K, Elsaid N, Levitt J, Chung PH, Somavarapu S, Jackson TL. 2012. Influence of molecular shape, conformability, net surface charge, and tissue interaction on transscleral macromolecular diffusion. Exp Eye Res 102:85–92.

20. Wilkins DK, Grimshaw SB, Receveur V, Dobson CM, Jones JA, Smith LJ. 1999. Hydrodynamic radii of native and denatured proteins measured by pulse field gradient NMR techniques. Biochemistry 38:16424–16431.

21. Tratta E, Pescina S, Padula C, Santi P, Nicoli S. 2014. In vitro permeability of a model protein across ocular tissues and effect of iontophoresis on the transscleral delivery. Eur J Pharm Biopharm 88:116–122.

22. Pescina S, Padula C, Santi P, Nicoli S. 2011. Effect of formulation factors on the trans-scleral iontophoretic and post-iontophoretic transport of a 40kDa dextran in-vitro. Eur J Pharm Sci 42:503–508.

23. Yim YS, Choi JS, Kim GT, Kim CH, Shin TH, Kim DG, Cheon J. 2012. A facile approach for the delivery of inorganic nanoparticles into the brain by passing through the blood–brain barrier (BBB). Chem Commun 48:61–63.

24. Rasband WS.1997–2014. ImageJ. Bethesda, Maryland: US National Institutes of Health. [Query:PE-Q1 to ALL] AU: Please check the presentation of Ref. 18 for correctness.

25. Nicoli S, Ferrari G, Quarta M, Macaluso C, Govoni P, Dallatana D, Santi P. 2009. Porcine sclera as a model of human sclera for in vitro transport experiments: Histology, SEM, and comparative permeability. Mol Vis 15:259–266.

26. Aihara M, Lindsey JD, Weinreb RN. 2001. Enhanced FGF-2 movement through human sclera after exposure to latanoprost. Invest Ophthalmol Vis Sci 42:2554–2559.

27. Amaral J, Fariss RN, Campos MM, RobisonWGJr, Kim H, Lutz R, Becerra SP. 2005. Transscleral-RPE permeability of PEDF and ovalbumin proteins: Implications for subconjunctival protein delivery. Invest Ophthalmol Vis Sci 46:4383–4392.

28. Wen H, Hao J, Li SK. 2013. Characterization of human sclera barrier properties for transscleral delivery of bevacizumab and ranibizumab. J Pharm Sci 102:892–903.

29. Maurice DM, Polgar J. 1977. Diffusion across the sclera. Exp Eye Res 25:577–582.

30. Cruysberg LP, Nuijts RM, Geroski DH, Gilbert JA, Hendrikse F, Edelhauser HF. 2005. The influence of intraocular pressure on the transscleral diffusion of high-molecular-weight compounds. Invest Ophthalmol Vis Sci 46:3790–3794.

31. Anderson OA, Jackson TL, Singh JK, Hussain AA, Marshall J. 2008. Human transscleral albumin permeability and the effect of topographical location and donor age. Invest Ophthalmol Vis Sci 49:4041–4045.

32. Chopra P, Hao J, Li SK. 2010. Iontophoretic transport of charged macromolecules across human sclera. Int J Pharm 388:107–113.

33. Ambati J, Canakis CS, Miller JW, Gragoudas ES, Edwards A, Weissgold DJ, Delori FC, Adamis AP. 2000. Diffusion of high molecular weight compounds through sclera. Invest Ophthalmol Vis Sci 41:1181–1185.

34. Huang D, Wang L, Dong Y, Pan X, Li G, Wu C. 2014. A novel technology using transscleral ultrasound to deliver protein loaded nanoparticles. Eur J Pharm Biopharm 88:104–115.

35. Pescina S, Antopolsky M, Santi P, Nicoli S, Murtomäki L. 2013. Effect of iontophoresis on the in vitro trans-scleral transport of three single stranded oligonucleotides. Eur J Pharm Sci 49:142–147.

36. Shuler RK, Dioguardi PK, Henjy C, Nickerson JM, Cruysberg LP, Edelhauser HF. 2004. Scleral permeability of a small, single-stranded oligonucleotide. J Ocul Pharm Ther 20:159–168.

37. Olsen TW, Edelhauser HF, Lim JI, Geroski DH. 1995. Human scleral permeability. Effects of age, cryotherapy, transscleral diode laser, and surgical thinning. Invest Ophthalmol Vis Sci 36:1893–1903.

38. Ahmed I, Gokhale RD, Shah MV, Patton TF. 1987. Physicochemical determinants of drug diffusion across the conjunctiva, sclera, and cornea. J Pharm Sci 76:583–586.

39. Nicoli S, Ferrari G, Quarta M, Macaluso C, Santi P. 2009. In vitro transscleral iontophoresis of high molecular weight neutral compounds. Eur J Pharm Sci 36:486–492.

40. Kim JW, Lindsey JD, Wang N, Weinreb RN. 2001. Increased human scleral permeability with prostaglandin exposure. Invest Ophthalmol Vis Sci 42:1514–1521.

41. Thrimawithana TR, Young SA, Bunt CR, Green CR, Alany RG. 2011. In-vitro and in-vivo evaluation of carrageenan/methylcellulose polymeric systems for transscleral delivery of macromolecules. Eur J Pharm Sci 44:399–409.

42. Boubriak OA, Urban JP, Akhtar S, Meek KM, Bron AJ. 2000. The effect of hydration and matrix composition on solute diffusion in rabbit sclera. Exp Eye Res 71:503–514.

43. Fattal E, Bochot A. 2006. Ocular delivery of nucleic acids: Antisense oligonucleotides, aptamers and siRNA. Ad Drug Deliv Rev 58:1203–1223.

44. Mandel M.1993. Some properties of polyelectrolyte solutions and the scaling approach. New York: Marcel Dekker.

45. Pescina S, Santi P, Ferrari G, Nicoli S. 2011. Trans-scleral delivery of macromolecules. Ther Deliv 2:1331–1349.

46. Wen H, Hao J, Li SK. 2010. Influence of permeant lipophilicity on permeation across human sclera. Pharm Res 27:2446–2456.

47. Cheruvu NPS, Kompella UB. 2006. Bovine and porcine transscleral solute transport: Influence of lipophilicity and the choroid-Bruch's layer. Invest Ophthalmol Vis Sci 47:4513–4522.

48. Lin CW, Wang Y, Challa P, Epstein DL, Yuan F. 2007. Transscleral diffusion of ethacrynic acid and sodium fluorescein. Mol Vis 13:243–251.

49. Gyenge CC, Tenstad O, Wiig H. 2003. In vivo determination of steric and electrostatic exclusion of albumin in rat skin and skeletal muscle. J Physiol 552:907–916.

50. Taylor AE, Parker JC. 2003. Intersitial exluded volumes: The effect of charge. J Physiol 553:333.

51. Kontturi AK, Kontturi K, Niinikoski P, Savonen A, Vuoristo M. 1992. The effective charge number and diffusion coefficient of cationic cytochrome c in aqueous solution. Acta Chem Scand 46:348–353.

52. Kontturi A-K, Kontturi K, Savonen A, Vuoristo M, Schiffrin DJ. 1993. Electrical migration in convective electrophoresis: Modelling and membrane separation of bovum serum albumin (BSA) and cytochrome c. J Chem Soc, Farad Trans 89:99–106.

53. Murtomaki L, Vainikka T, Pescina S, Nicoli S. 2013. Drug adsorption on bovine and porcine sclera studied with streaming potential. J Pharm Sci 102:2264–2272.

54. Raiman J, Hanninen K, Kontturi K, Murtomaki L, Hirvonen J. 2003. Drug adsorption in human skin: A streaming potential study. J Pharm Sci 92:2366–2372.

55. Waldbillig RJ, Arnold DR, Fletcher RT, Chader GJ. 1990. Insulin and IGF-1 binding in chick sclera. Invest Ophthalmol Vis Sci 31:1015–1022.

56. Dubey S, Kalia YN. 2014. Understanding the poor iontophoretic transport of lysozyme across the skin: When high charge and high electrophoretic mobility are not enough. J Control Release 183:35–42.

57. Chopra P, Hao J, Li SK. 2012. Sustained release micellar carrier systems for iontophoretic transport of dexamethasone across human sclera. J Control Release 160:96–104.

58. Hussain AA, Starita C, Hodgetts A, Marshall J. 2010. Macromolecular diffusion characteristics of ageing human Bruch's membrane: Implications for age-related macular degeneration (AMD). Exp Eye Res 90:703–710.

59. Bernstein MH, Hollenberg MJ. 1965. Fine structure of the choriocapillaris and retinal capillaries. Invest Ophthalmol 4:1016–1025.

60. Starita C, Hussain AA, Patmore A, Marshall J. 1997. Localization of the site of major resistance to fluid transport in Bruch's membrane. Invest Ophthalmol Vis Sci 38:762–767.

61. Moore DJ, Clover GM. 2001. The effect of age on the macromolecular permeability of human Bruch's membrane. Invest Ophthalmol Vis Sci 42:2970–2975.

62. Cankova Z, Huang J-D, Kruth HS, Johnson M. 2011. Passage of low-density lipoproteins through Bruch's membrane and choroid. Exp Eye Res 93:947–955.

63. Cheruvu NPS, Amrite AC, Kompella UB. 2008. Effect of eye pigmentation on transscleral drug delivery. Invest Ophthalmol Vis Sci 49:333–341.

64. Pitkanen L, Ranta V-P, Moilanen A, Urtti A. 2007. Binding of betaxolol, metoprolol and oligonucleotides to synthetic and bovine ocular melanin, and prediction of drug binding to melanin in human choroid-retinal pigment epithelium. Pharm Res 24:2063–2070.

65. Pescina S, Santi P, Ferrari G, Padula C, Cavallini P, Govoni P, Nicoli S. 2012. Ex vivo models to evaluate the role of ocular melanin in trans-scleral drug delivery. Eur J Pharm Sci 46:475–483.

66. Dastjerdi MH, Sadrai Z, Saban DR, Zhang Q, Dana R. 2011. Corneal penetration of topical and subconjunctival bevacizumab. Invest Ophthalmol Vis Sci 52:8718–8723.

67. Ferrari G, Bignami F, Giacomini C, Franchini S, Rama P. 2013. Safety and efficacy of topical infliximab in a mouse model of ocular surface scarring. Invest Ophthalmol Vis Sci 54:1680–1688.

68. Al-Mahmood S, Colin S, Farhat N, Thorin E, Steverlynck C, Chemtob S. 2009. Potent in vivo antiangiogenic effects of GS-101 (5'-TATCCGGAGGGCTCGCCATGCTGCT-3'), an antisense oligonucleotide preventing the expression of insulin receptor substrate-1. J Pharmacol Exp Ther 329:496–504.

69. Meek KM, Leonard DW. 1993. Ultrastructure of the corneal stroma: A comparative study. Biophys J 64:273–280.

70. Berdugo M, Valamanesh F, Andrieu C, Klein C, Courtois Y, Behar-Cohen F. 2003. Delivery of antisense oligonucleotide to the cornea by iontophoresis. Antisense Nucleic Acid Drug Dev 13:107–114.

71. Brereton HM, Taylor SD, Farrall A, Hocking D, Thiel MA, Tea M, Coster DJ, Williams KA. 2005. Influence of format on in vitro penetration of antibody fragments through porcine cornea. Br J Ophthalmol 89:1205–1209.

72. Ottiger M, Thiel MA, Feige U, Lichtlen P, Urech DM. 2009. Efficient intraocular penetration of topical anti-TNF-alpha single-chain antibody (ESBA105) to anterior and posterior segment without penetration

enhancer. Invest Ophthalmol Vis Sci 50:779–786.

73. Thiel MA, Coster DJ, Standfield SD, Brereton HM, Mavrangelos C, Zola H, Taylor S, Yusim A, Williams KA. 2002. Penetration of engineered antibody fragments into the eye. Clin Exp Immunol 128:67–74.

74. Charalel RA, Engberg K, Noolandi J, Cochran JR, Frank C, Ta CN. 2012. Diffusion of protein through the human cornea. Ophthalmic Res 48:50–55.

75. Nakamura T, Yamada M, Teshima M, Nakashima M, To H, Ichikawa N, Sasaki H. 2007. Electrophysiological characterization of tight junctional pathway of rabbit cornea treated with ophthalmic ingredients. Biol Pharm Bull 30:2360–2364.

76. Nemoto E, Takahashi H, Kobayashi D, Ueda H, Morimoto Y. 2006. Effects of poly-L-arginine on the permeation of hydrophilic compounds through surface ocular tissues. Biol Pharm Bull 29:155–160.

77. Spitznas M, Reale E. 1975. Fracture faces of fenestrations and junctions of endothelial cells in human choroidal vessels. Invest Ophthalmol 14:98–107.

78. Rieke ER, Amaral J, Becerra SP, Lutz RJ. 2010. Sustained subconjunctival protein delivery using a thermosetting gel delivery system. J Ocul Pharm Ther 26:55–64.

79. Kim SH, Csaky KG, Wang NS, Lutz RJ. 2008. Drug elimination kinetics following subconjunctival injection using dynamic contrast-enhanced magnetic resonance imaging. Pharm Res 25:512–520.

80. Ban Y, Rizzolo LJ. 1997. A culture model of development reveals multiple properties of RPE tight junctions. Mol Vis 3:18.

81. Pitkanen L, Ranta V-P, Moilanen A, Urtti A. 2005. Permeability of retinal pigment epithelium: Effects of permeant molecular weight and lipophilicity. Invest Ophthalmol Vis Sci 46:641–646.